Journal of Applied Mathematics and Physics, 2025, 13(7), 2820-2835
https://www.scirp.org/journal/jamp
ISSN Online: 2327-4379
ISSN Print: 2327-4352

Wave-Domain Near-Field Acoustic Error Sensing Strategy for Active Control of Radiated Sound in a Free Space

Shengping Fan, Yifan Wang, Linyong Li

Guangdong Electric Power Science Academe, Guangdong, China
Email: 13926035445@163.com, 846718455@qq.com, 897727594@qq.com

How to cite this paper: Fan, S.P., Wang, Y.F. and Li, L.Y. (2025) Wave-Domain Near-Field Acoustic Error Sensing Strategy for Active Control of Radiated Sound in a Free Space. *Journal of Applied Mathematics and Physics*, **13**, 2820-2835.
https://doi.org/10.4236/jamp.2025.138161

Received: July 25, 2025
Accepted: August 26, 2025
Published: August 29, 2025

Abstract

The challenges of near-field acoustic error sensing lie in the measurement of the total radiated sound power and the optimization of error sensor configuration which depends on the information of secondary sources configuration. The wave-domain strategy is proposed. In the background of the global control of radiated sound in a two-dimensional free space, the active control cost function is formulated in the cylindrical harmonic domain using the exterior sound field reproduction theory with higher order microphones as error sensors. The equivalence with the minimization of the acoustic power is indicated by deriving the optimal secondary source strengths expression. Optimal configuration parameters of error sensors are investigated via simulations. Under the circumstances of the same electroacoustic device configuration, performances of the proposed strategy are compared with those of the conventional pressure matching strategy. Results show that better attenuation levels and system performances are obtained when error sensors and secondary sources are very close. In addition, the proposed strategy decouples the configurations of error sensors and secondary sources, which simplifies the optimization of error sensor configurations.

Keywords

Error Sensing, Active Noise Control, Wave Domain

1. Introduction

In free space active noise control (ANC), in order to achieve noise reduction in the whole space range, the distance between the secondary sound source and the primary sound source needs to be less than half a wavelength [1]. The near-field

acoustic error sensing strategy is also a key issue. The ANC cost function is constructed by using the sound field information picked up by the error sensor to reduce the total radiation sound power [2]. The secondary path delay of the near-field strategy is short, which is conducive to system stability. The distance between the error sensor and the secondary sound source is close, which facilitates the realization of a compact system. It is suitable for noise radiation control application scenarios such as transformers [3]-[5] and axial cooling fans [6], especially mobile noise sources (such as a trailer in motion [7]). However, there are many difficulties in the near-field strategy, mainly in finding the appropriate cost function and the optimal layout of the error sensor. Qiu *et al.* [8] compared eight near-field strategies, and found that when the error sensor is very close to the secondary sound source, the sum of the average radial active sound intensity of the finite point is the optimal strategy, but the sound intensity sensing will encounter many difficulties in practical applications [2]. At present, the commonly used method is to use the square sum of the sound pressure of the finite point in the microphone sampling space as the cost function. The essence is to realize the inverse matching of the primary sound pressure at the error point (called the sound pressure matching strategy in this paper). However, near-field microphones cannot effectively obtain sound power information at low frequencies or when the noise source size is large [9]. The layout of the error sensor also greatly influences the strategy's noise reduction effect. Although there is an analytical optimal position [10], it is not easy to determine in practice, and the position deviation will greatly reduce the noise reduction effect [11]. The optimization method mostly uses optimization search [12]-[14], but it needs to measure the acoustic transmission impedance (ATI) of the secondary sound source in advance, that is, it depends on the layout information of the secondary sound source. The two are coupled with each other and it is difficult to obtain the optimal result. The sound field can be expanded by the basis function, and the sound pressure at any point in the sound field can be approximated by the finite-order sound field coefficient. In recent years, the use of higher order microphone (HOM) to pick up the sound field for spatial sound field reconstruction [15]-[17] and other research has become a hot spot. At the same time, the sound field decomposition theory is introduced into ANC, and the wave-domain ANC is proposed. The corresponding adaptive algorithm [18] and the secondary path modeling method [19] are explored for the internal sound field problem (that is, all sound sources and obstacles are located outside the examination area). For the external sound field problems involved in active control of acoustic radiation (*i.e.*, areas other than all sound sources and obstacles), related technologies can be used to provide new ideas for near-field acoustic error sensing. In this paper, a near-field acoustic error sensing strategy in wave domain is proposed. Taking two-dimensional free space acoustic radiation as the object, HOM is used to pick up the error signal, which can effectively map the radiated sound power information. The optimization of the layout of the error sensor only needs to consider whether it accurately estimates the sound field

coefficient, without the need for specific secondary source layout information, which can greatly simplify the debugging work. Although the two-dimensional case is considered, the problem is more idealized, but the sound field analysis is simple and convenient to study the relevant laws, and the strategy is easy to extend to the three-dimensional case.

2. Wave-Domain Near-Field Acoustic Error Sensing Strategy

The use of multiple line source secondary sound sources to control the acoustic radiation of multiple line source primary sound sources in two-dimensional free space is discussed. Firstly, the model is described. Then, the sound field coefficient is obtained by HOM, and the sound field coefficient of the secondary sound field is represented by the intensity of the secondary sound source. Finally, the ANC cost function is given, and its adaptive algorithm is briefly introduced.

2.1. Model Description

The geometric representation of the problem under consideration is shown in **Figure 1(a)**. The L secondary sound sources used to cancel the primary noise are evenly distributed on the circumference with a radius of R_{secs}, close to the primary sound source. The radius R_s of the circular region Ω_{in} that surrounds all sound sources satisfies $R_s \geq R_{\text{secs}}$ (For convenience, let $R_s = R_{\text{secs}}$ in the examples of this paper).Outside the region Ω_{in}, multiple HOMs are used to pick up the sound field information. HOM uses an open circular microphone array with a radius of R. The layout of the HOM can be arbitrary, which is convenient

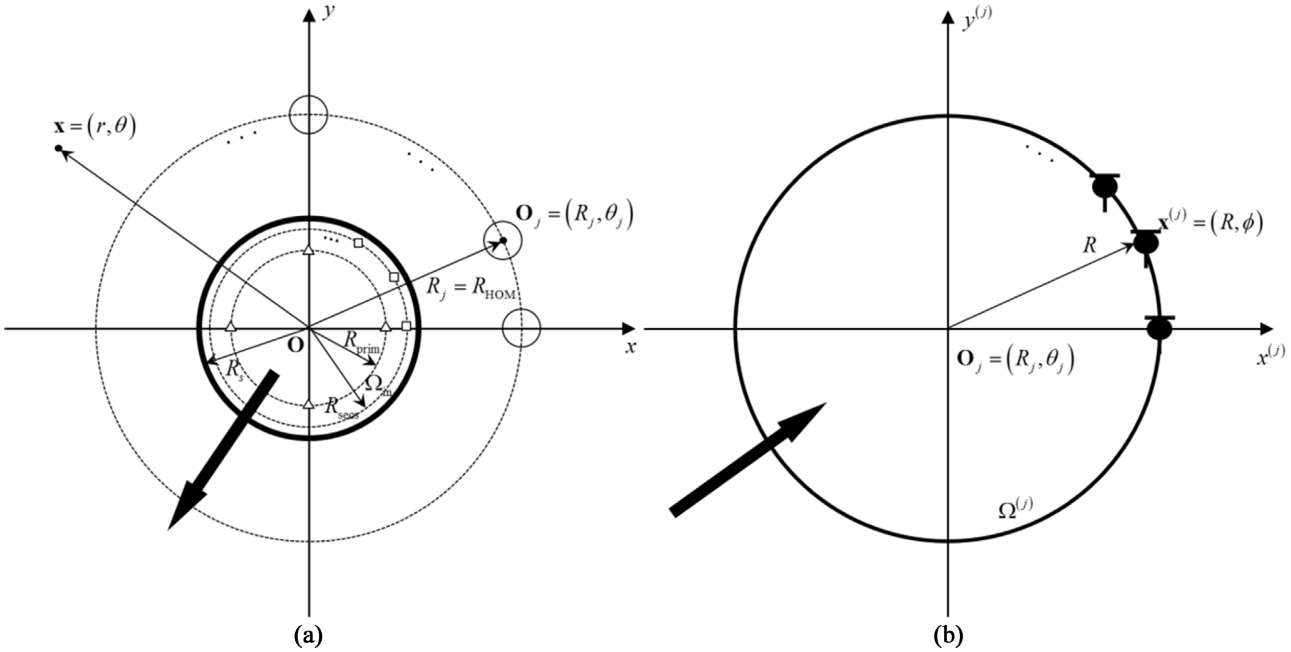

(△: Primary sound source, ☑: secondary sound source, ○: HOM, Coarse arrow: Sound wave).

Figure 1. Geometrical representation of active control model for two-dimensional free space acoustic radiation. (a) Global coordinate system; (b) The local coordinate system of the jth HOM.

to express. It is evenly distributed on the circumference with a radius of $R_j = R_{\mathrm{HOM}}$ ($j = 1, 2, \ldots, J$), and the order of each HOM is the same.

2.2. Pickup of Two-Dimensional External Sound Field

For the local circular region $\Omega^{(j)}$ of the jth ($j = 1, 2, \ldots, J$) HOM, a local polar coordinate system is established, as shown in **Figure 1(b)**. Since the sound source is located outside the region $\Omega^{(j)}$, it can be regarded as an internal sound field problem. The sound pressure at any microphone position $\mathbf{x}^{(j)} = (R, \phi)$ on the HOM can be expanded by the cylindrical harmonic function as:

$$p\left(\mathbf{x}^{(j)}, k\right) \approx \sum_{n=-N}^{N} \alpha_n^{(j)}(k) \mathrm{J}_n(kR) e^{in\phi} \tag{1}$$

where k is the wave number, $\mathrm{J}_n(\cdot)$ denotes the n-th order column Bessel function, $\alpha_n^{(j)}(k)$ is the local acoustic field coefficient relative to the origin $\mathbf{O}_j = (R_j, \theta_j)$ of the local coordinate system, and the truncation order $N = \lceil ekR/2 \rceil$, $\lceil \bullet \rceil$ represents the upward rounding. In order to avoid spatial aliasing, the number of microphones is set to $M = 2N+1$. The above formula is written in matrix form as

$$\mathbf{p}_j = \mathbf{Y}_j \boldsymbol{\alpha}_j \tag{2}$$

In the formula, $\mathbf{p}_j$ is the pick-up sound pressure vector of $M \times 1$, $\boldsymbol{\alpha}_j$ is the local sound field coefficient vector of $(2N+1) \times 1$, $\mathbf{Y}_j$ is the matrix of $M \times (2N+1)$ (here $M = 2N+1$, so it is a square matrix), element $\left[\mathbf{Y}_j\right]_{\mu,\nu} = \mathrm{J}_n(kR) e^{in\phi_m}$, where $\mu = m$, $\nu = n + N + 1$.

Since the sound sources are located in the region Ω_{in}, the sound field outside the region Ω_{in} is considered as the external sound field. The sound pressure $\mathbf{x} = (r, \theta)$ at any point can be expanded as (time factor $e^{i\omega t}$)

$$p(\mathbf{x}, k) \approx \sum_{m=-N_s}^{N_s} \beta_m(k) \mathrm{H}_m^{(2)}(kr) e^{im\theta} \tag{3}$$

where $\mathrm{H}_m^{(2)}(\cdot)$ is the second kind of cylindrical Hankel function of order m, $\beta_m(k)$ is the external sound field coefficient (hereinafter referred to as the sound field coefficient), and the truncation order is $N_s = \lceil ekR_s/2 \rceil$, which is expressed in matrix form.

$$\mathbf{p} = \mathbf{H}\boldsymbol{\beta} \tag{4}$$

In the formula, $\mathbf{p}$ is the $JM \times 1$ picking sound pressure vector, and $\boldsymbol{\beta}$ is the sound field coefficient vector of $(2N_s+1) \times 1$.

The J group local acoustic field coefficient $\left\{\boldsymbol{\alpha}_j\right\}_{j=1}^{J}$ was obtained by using the HOM array, and the Graf addition theorem of the cylindrical Hankel function was used [20].

$$\mathrm{H}_m^{(2)}(kr) e^{im\theta} = \sum_{n=-\infty}^{\infty} \mathrm{H}_{n-m}^{(2)}\left(kR_j\right) \mathrm{J}_n(kR) e^{in\phi} e^{i(m-n)(\pi+\theta_j)} \tag{5}$$

The relationship between the local acoustic field coefficient $\boldsymbol{\alpha}_j$ and the acoustic field coefficient $\boldsymbol{\beta}$ of group j can be obtained.

$$\alpha_n^{(j)}(k) \approx \sum_{m=-N_s}^{N_s} \beta_m(k) \mathrm{H}_{m-n}^{(2)}(kR_j) e^{i(m-n)\theta_j} \tag{6}$$

Written in matrix form as

$$\boldsymbol{\alpha}_j = \mathbf{T}_j \boldsymbol{\beta} \tag{7}$$

where $\mathbf{T}_j$ is the matrix of $(2N+1)\times(2N_s+1)$, element $\left[\mathbf{T}_j\right]_{\mu,\nu} = \mathrm{H}_{m-n}^{(2)}(kR_j) e^{i(m-n)\theta_j}$ while $\mu = n+N+1$, $\nu = m+N_s+1$.

Combining the local sound field coefficients of group J with Equations (2), (4) and (7), it can be obtained that

$$\mathbf{H} = \begin{bmatrix} \mathbf{Y}_1\mathbf{T}_1 \\ \mathbf{Y}_2\mathbf{T}_2 \\ \vdots \\ \mathbf{Y}_J\mathbf{T}_J \end{bmatrix}_{JM\times(2N_s+1)} \tag{8}$$

It should be noted that in order to guarantee the unique solution of (4), the equations need to be overdetermined, that is, $JM \geq 2N_s+1$.

In general, using the HOM array to pick up the sound field pressure $\mathbf{p}$, the sound field coefficient can be solved by the least square method.

$$\boldsymbol{\beta} = \left(\mathbf{H}^H\mathbf{H}\right)^{-1}\mathbf{H}^H\mathbf{p} \tag{9}$$

$(\bullet)^H$ denotes conjugate transpose. If $\mathbf{H}$ is morbid, regularization needs to be applied.

2.3. Wave Domain Representation of Two-Dimensional Secondary Sound Field

Suppose that the intensity of the lth secondary sound source is $q_l(k)$, then the secondary sound pressure at any point $\mathbf{x} = (r,\theta)$ can be expressed as

$$p^{(s)}(\mathbf{x},k) = \sum_{l=1}^{L} q_l(k) z_l(r,\theta,k) \tag{10}$$

The superscript (s) denotes the secondary sound field, and $z_l(r,\theta,k)$ denotes the ATI between the lth secondary sound source and the observation point $\mathbf{x} = (r,\theta)$. For two-dimensional free fields, there are [21]

$$z_l(r,\theta,k) = z_0 \mathrm{H}_0^{(2)}\left(k\left\|\mathbf{x}_l - \mathbf{x}\right\|\right) \tag{11}$$

where $z_0 = \rho ck/4$, $\mathbf{x}_l = (r_l,\theta_l)$ is the lth position of the secondary sound source.

In the frequency domain, the ATI between two points is numerically equal to the sound pressure generated at the other point when the intensity of the unit sound source ($q = 1$ m²/s) is applied at one point, so here $z_l(r,\theta,k)$ can be expanded by the cylindrical harmonic function as follows

$$z_l(r,\theta,k) \approx \sum_{m=-N_s}^{N_s} \gamma_{ml}(k) \mathrm{H}_m^{(2)}(kr) e^{im\theta} \tag{12}$$

$\gamma_{ml}(k)$ is the ATI coefficient, which is independent of the position of the receiving point. Applying the following addition theorem [20].

$$\mathrm{H}_0^{(2)}\left(k\left\|\mathbf{x}_l-\mathbf{x}\right\|\right)=\sum_{m=-\infty}^{\infty}\mathrm{J}_m\left(kr_l\right)\mathrm{H}_m^{(2)}\left(kr\right)e^{im(\theta-\theta_l)},\quad r>r_l \tag{13}$$

Recombine formula (11) and (12) could get

$$\gamma_{ml}(k)=z_0\,\mathrm{J}_m\left(kr_l\right)e^{-im\theta_l} \tag{14}$$

With formula (3), (12)& (14), the relationship between the sound field coefficient $\boldsymbol{\beta}_s$ of the secondary sound field and the secondary sound source intensity $\mathbf{q}_s$ can be obtained.

$$\beta_m^{(s)}(k)=\sum_{l=1}^{L}q_l(k)\gamma_{ml}(k),\quad m=-N_s,\ldots,N_s \tag{15}$$

written in matrix would be

$$\boldsymbol{\beta}_s=\boldsymbol{\Gamma}\mathbf{q}_s \tag{16}$$

$\boldsymbol{\Gamma}$ is the ATI coefficient matrix of $(2N_s+1)\times L$, element $\left[\boldsymbol{\Gamma}\right]_{\mu,\nu}=z_0\,\mathrm{J}_m\left(kr_l\right)e^{-im\theta_l}$, where $\mu=m+N_s+1$, $\nu=l$. It must be emphasized that $\boldsymbol{\Gamma}$ is only related to the secondary sound source layout, and there is no error sensor layout information.

It should be noted that due to the clear characteristics of free space acoustic transmission, the ATI coefficient matrix here can be given by analytical expression. In practice, the secondary path modeling method can be used to excite the secondary sound source in turn with white noise, and the sound field coefficient of the sound field obtained by HOM is the ATI coefficient of the secondary sound source.

2.4. Active Control Cost Function

After expanding the sound field in the cylindrical harmonic function domain, it is most intuitively to minimize the sum of the square of the sound field coefficient $\boldsymbol{\beta}_t^H\boldsymbol{\beta}_t$ of the total sound field after control. Substituting it into $\boldsymbol{\beta}_t=\boldsymbol{\beta}_p+\boldsymbol{\beta}_s$ and formula (16), the cost function can be expressed as

$$J_{\mathrm{WD}}\left(\mathbf{q}_s\right)=\mathbf{q}_s^H\left(\boldsymbol{\Gamma}^H\boldsymbol{\Gamma}\right)\mathbf{q}_s+\mathbf{q}_s^H\left(\boldsymbol{\Gamma}^H\boldsymbol{\beta}_p\right)+\left(\boldsymbol{\beta}_p^H\boldsymbol{\Gamma}\right)\mathbf{q}_s+\boldsymbol{\beta}_p^H\boldsymbol{\beta}_p \tag{17}$$

Since $\boldsymbol{\Gamma}^H\boldsymbol{\Gamma}$ is a symmetric positive definite matrix, the unique optimal secondary source intensity vector can be found to be

$$\mathbf{q}_s=-\left(\boldsymbol{\Gamma}^H\boldsymbol{\Gamma}\right)^{-1}\boldsymbol{\Gamma}^H\boldsymbol{\beta}_p \tag{18}$$

Then the near-field analysis method [10] can be used to calculate the total radiation sound power W_t of the primary and secondary sound sources after control (the next section), and the noise reduction AL_W of the radiation sound power is obtained.

In practice, when the wave domain control is realized, the sound pressure of the sound field is picked up by the HOM array and input into the adaptive controller.

Firstly, the sound pressure signal is transformed into the wave domain by using the wave domain conversion algorithm to obtain the sound field coefficient. Then, the secondary signal output is adjusted by the wave domain adaptive algorithm. The secondary sound source generates a secondary sound field, which is offset by the primary sound field [18].

3. Relationship with Acoustic Power Minimization Strategy

The best state of active control of acoustic radiation is to minimize the radiated sound power after active control. Therefore, people often use the sound power minimization strategy and its results as a benchmark to measure the performance of the acoustic error sensing strategy. In this section, the relationship between the wave domain strategy and the radiated sound power minimization strategy is derived from the perspective of the secondary sound source intensity vector.

Using the near-field analysis method, the total radiated sound power can be obtained by calculating the actual sound power output of the primary and secondary sound sources.

$$W_t = \mathbf{q}_s^H \mathbf{A}\mathbf{q}_s + \mathbf{q}_s^H \mathbf{b} + \mathbf{b}^H \mathbf{q}_s + C \tag{19}$$

The meanings of $\mathbf{A}$, $\mathbf{b}$ and C in the formula are given in reference [2]. The analytical formula of the optimal secondary sound source intensity is obtained easily.

$$\mathbf{q}_s^{\text{opt}} = -\mathbf{A}^{-1}\mathbf{b} \tag{20}$$

For the examined model, the elements of $\mathbf{A}$ and $\mathbf{b}$ in Equation (2) are

$$[\mathbf{A}]_{l,l'} = \frac{z_0}{2} \mathrm{J}_0\left(kd_{sl,sl'}\right), \quad l = 1,...,L, \quad l' = 1,...,L \tag{21}$$

$$[\mathbf{b}]_l = \frac{z_0}{2} \sum_{\ell=1}^{K} \mathrm{J}_0\left(kd_{sl,p\ell}\right) q_{p\ell}, \quad l = 1,...,L \tag{22}$$

In the formula, $d_{sl,sl'}$ represents the distance between the lth secondary sound source and the l'th secondary sound source, $d_{sl,p\ell}$ represents the distance between the lth secondary sound source and the ℓth primary sound source, and $q_{p\ell}$ represents the intensity of the ℓth primary sound source.

Comparing Equations (18) and (20), the two forms are the same. The element of easy derivation $\mathbf{\Gamma}^H\mathbf{\Gamma}$ is expressed as

$$\left[\mathbf{\Gamma}^H\mathbf{\Gamma}\right]_{l,l'} = z_0^2 \sum_{m=-N_s}^{N_s} \mathrm{J}_m\left(kr_l\right)\mathrm{J}_m\left(kr_{l'}\right)\cos m\left(\theta_l - \theta_{l'}\right), \quad l = 1,...,L, \quad l' = 1,...,L \tag{23}$$

For $\mathbf{\Gamma}^H\boldsymbol{\beta}_p$, assuming that there is no error in the estimation of the sound field coefficient, that is, $\boldsymbol{\beta}_p$ is equal to the theoretical value $\boldsymbol{\beta}_0$, the element expression of t $\mathbf{\Gamma}^H\boldsymbol{\beta}_0$ is

$$\left[\mathbf{\Gamma}^H\boldsymbol{\beta}_0\right]_l = z_0^2 \sum_{\ell=1}^{K} \sum_{m=-N_s}^{N_s} \mathrm{J}_m\left(kr_l\right)\mathrm{J}_m\left(kr_{p\ell}\right)\cos m\left(\theta_l - \theta_{p\ell}\right) q_{p\ell}, \quad l = 1,...,L \tag{24}$$

where $\left(r_{p\ell}, \theta_{p\ell}\right)$ ($\ell = 1,...,K$) represents the position of the primary sound source.

By Neumann addition theorem [20]

$$\mathrm{J}_0\left(kd\right)=\sum_{m=-\infty}^{\infty}\mathrm{J}_m\left(kr_1\right)\mathrm{J}_m\left(kr_2\right)\cos m\left(\theta_1-\theta_2\right) \tag{25}$$

In the formula, d is the distance between $\left(r_1,\theta_1\right)$ and $\left(r_2,\theta_2\right)$, combined with the above formula, the formula (21) and the formula (23) and the formula (22) and the formula (24) are compared respectively, ignoring the constants $z_0/2$ and z_0^2 (which will be eliminated in the operation), it is easy to see that when $N_s\to+\infty$, there are $\left(2/z_0\right)\mathbf{A}=\left(1/z_0^2\right)\mathbf{\Gamma}^H\mathbf{\Gamma}$, $\left(2/z_0\right)\mathbf{b}=\left(1/z_0^2\right)\mathbf{\Gamma}^H\boldsymbol{\beta}_0$, and then $\mathbf{q}_s=\mathbf{q}_s^{\mathrm{opt}}$. In other words, if there is no coefficient order truncation and coefficient estimation error, the wave domain strategy is equivalent to the radiated sound power minimization strategy [22] [23].

However, in practice, due to the existence of coefficient order truncation and coefficient estimation error, there is a loss of noise reduction in the wave domain strategy. The former determines the extent to which the wave-domain strategy can achieve the optimal noise reduction AL_W^{opt}, that is, the noise reduction upper limit AL_{W0}; the latter determines the actual noise reduction AL_W.

4. The Influence of Error Sensor Configuration Parameters on Noise Reduction

As an error sensor, the HOM array 's configuration parameters affect the accuracy of the coefficient estimation, which in turn affects the noise reduction. This section lists the configuration parameters and explains the relationship between some parameters; two evaluation quantities-coefficient estimation error and relative noise reduction loss are defined, and the relationship between them is explored by simulating different configuration parameters. At the same time, the influence of each parameter on the two is discussed, and the optimal configuration of the error sensor is obtained.

4.1. Configuration Parameter

Assuming that the microphone performance is ideal, the accuracy of the sound field coefficient estimated by the HOM array will be affected by the single HOM configuration, the HOM array layout, and the wave domain conversion algorithm. Among them, the single HOM configuration mainly involves its order N and radius R. The HOM array layout mainly includes the number of HOM J and the position $\mathbf{O}_j=\left(R_j,\theta_j\right)$. For the convenience of expression, it is assumed that the HOM array is evenly distributed on the circumference from $\mathbf{O}_1=\left(R_{\mathrm{HOM}},0\right)$, so the position only involves R_{HOM}. The wave-domain conversion algorithm uses the method described in section 2.2, that is, formula (9).

Since the overdetermined condition $JM\geq 2N_s+1$ needs to be satisfied, the relationship between J and N can be obtained as

$$N=\left\lceil\frac{2\pi eR_s f+c}{2c\mu J}-\frac{1}{2}\right\rceil \tag{26}$$

$$J = \left\lceil \frac{2\pi e R_s f + c}{c\mu(2N+1)} \right\rceil \tag{27}$$

In the formula, the μ oversampling factor is used to make a more accurate estimation near the frequency f. The value is obtained by experience, generally 0.6 - 1, and 0.75 is selected for the example in this paper. It can be seen that for the same frequency, the more HOM, the smaller the order required; for the same number of HOMs, if you want to pick up a higher frequency, you need to increase the order. After determining N, the radius $R = cN / \pi ef$ of HOM is obtained by $N = \lceil ekR / 2 \rceil$.

4.2. Coefficient Estimation Error and Relative Noise Reduction Loss

Define the coefficient estimation error $E_{\boldsymbol{\beta}}$ as follows

$$E_{\boldsymbol{\beta}} = \frac{\left(\boldsymbol{\beta}_0 - \boldsymbol{\beta}_p\right)^H \left(\boldsymbol{\beta}_0 - \boldsymbol{\beta}_p\right)}{\boldsymbol{\beta}_0^H \boldsymbol{\beta}_0} \tag{28}$$

In order to improve the noise reduction effect, the HOM array needs to pick up the sound field information more accurately, that is, E is small.

If the truncation effect is not considered, that is, assuming $AL_W^{\text{opt}} = AL_{W0}$, the loss of the actual noise reduction AL_W relative to AL_W^{opt} is defined as the relative noise reduction loss Δ, and the expression is

$$\Delta = \frac{AL_W^{\text{opt}} - AL_W}{AL_W^{\text{opt}}} \tag{29}$$

In order to examine the relationship between the relative noise reduction loss Δ and the coefficient estimation error $E_{\boldsymbol{\beta}}$, the number J of HOM and the position R_{HOM} are selected as independent variables. The order N and the radius R are determined by the number J; the $E_{\boldsymbol{\beta}}$ and the corresponding Δ in each case are calculated. It is assumed that the primary sound field is generated by four line sources with coordinates $(1,0)$, $(-1,0)$, $(0,1)$ and $(0,-1)$, and the intensity is 1 m/s^3. $R_s = 1 + \lambda/10$, λ is wavelength. J maintains 40 values. R_{HOM} includes 2 parts: from $R_s + R + \lambda/1000$ to $R_s + R + \lambda/4$, uniformly select 20 values; from $R_s + R + \lambda/4$ to $R_s + R + \lambda$, uniformly select 4 values (exclude $R_s + R + \lambda/4$), which lead to total 960 group of cases. The first five-order harmonic frequencies with a fundamental frequency of 100 Hz are calculated. The number of secondary sound sources is set to $L = 2N_s + 1$, and for these 5-order harmonics, it is calculated to be 9, 13, 19, 23 and 29, respectively.

Figure 2 shows the $E_{\boldsymbol{\beta}}$ and Δ of the corresponding 960 groups at five harmonic frequencies. It can be seen that the smaller the $E_{\boldsymbol{\beta}}$, the smaller the Δ, showing a nonlinear relationship. The curve trends of each harmonic frequency are the same, but there are differences. If $E_{\boldsymbol{\beta}}$ exceeds 0.2, the noise reduction will lose more than 80%. If you want to lose no more than 20 %, you basically need to reach the $E_{\boldsymbol{\beta}}$ to 0.0001 order of magnitude.

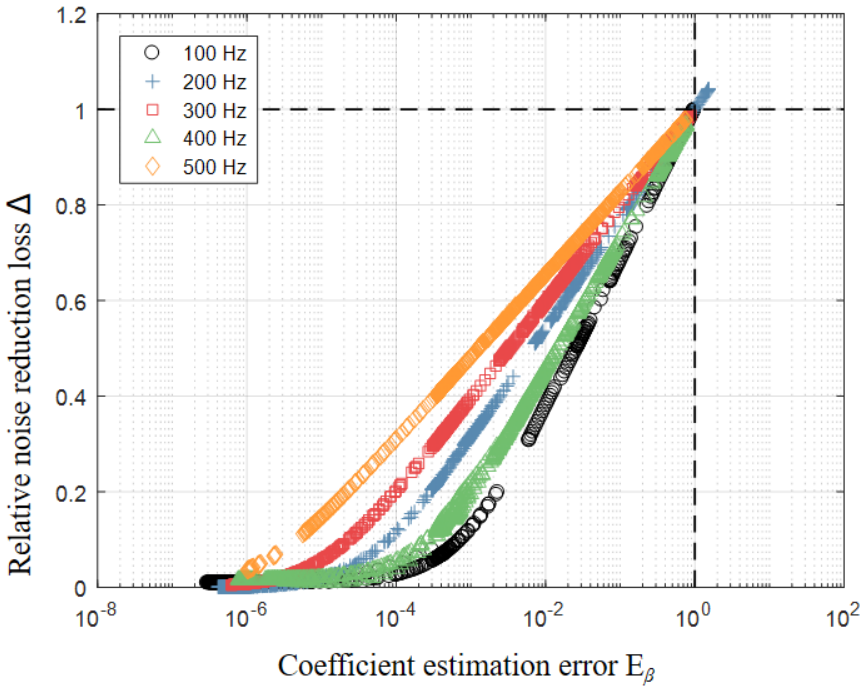

Figure 2. Relationship between coefficient estimation error and relative noise reduction loss

4.3. Optimal Configuration of Error Sensor

The influence of configuration parameters on coefficient estimation error and noise reduction is discussed. **Figure 3** shows the relationship between the total number of microphones JM and the order N of HOM with the coefficient estimation error E_β and the noise reduction AL_W at 100 Hz and 500 Hz, respectively. These two frequencies are selected because the far-field sound pressure distribution of the primary sound field is approximately non-directional at 100 Hz, and has complex directivity at 500 Hz, which is representative.

From **Figure 3**, it is clear that N and JM have the same effect on E_β and AL_W, respectively. AL_W has no obvious relationship with JM, even for the same N. N has a great influence on AL_W, and the smaller N is, the larger AL_W is. When $N=0$, the noise reduction effect is the best, close to the optimal noise reduction AL_W^{opt}. At this time, increasing J, AL_W does not increase significantly, but it will be affected by the HOM position R_{HOM}. In **Figure 3**, the color of the triangle mark representing $N=0$ from shallow to deep indicates that R_{HOM} is getting larger and larger. According to the observation, AL_W increases first and then tends to be stable with the increase of R_{HOM}.

In summary, the configuration of the HOM array as an error sensor should select the 0-order HOM, that is, a microphone ; the choice of the number J satisfies the minimum value of the overdetermined condition, which can be obtained by formula (27). When the layout is uniform on the circumference, the radius R_{HOM} cannot be too small, that is, the microphone cannot be too close to the secondary sound source, otherwise the effect will be lost.

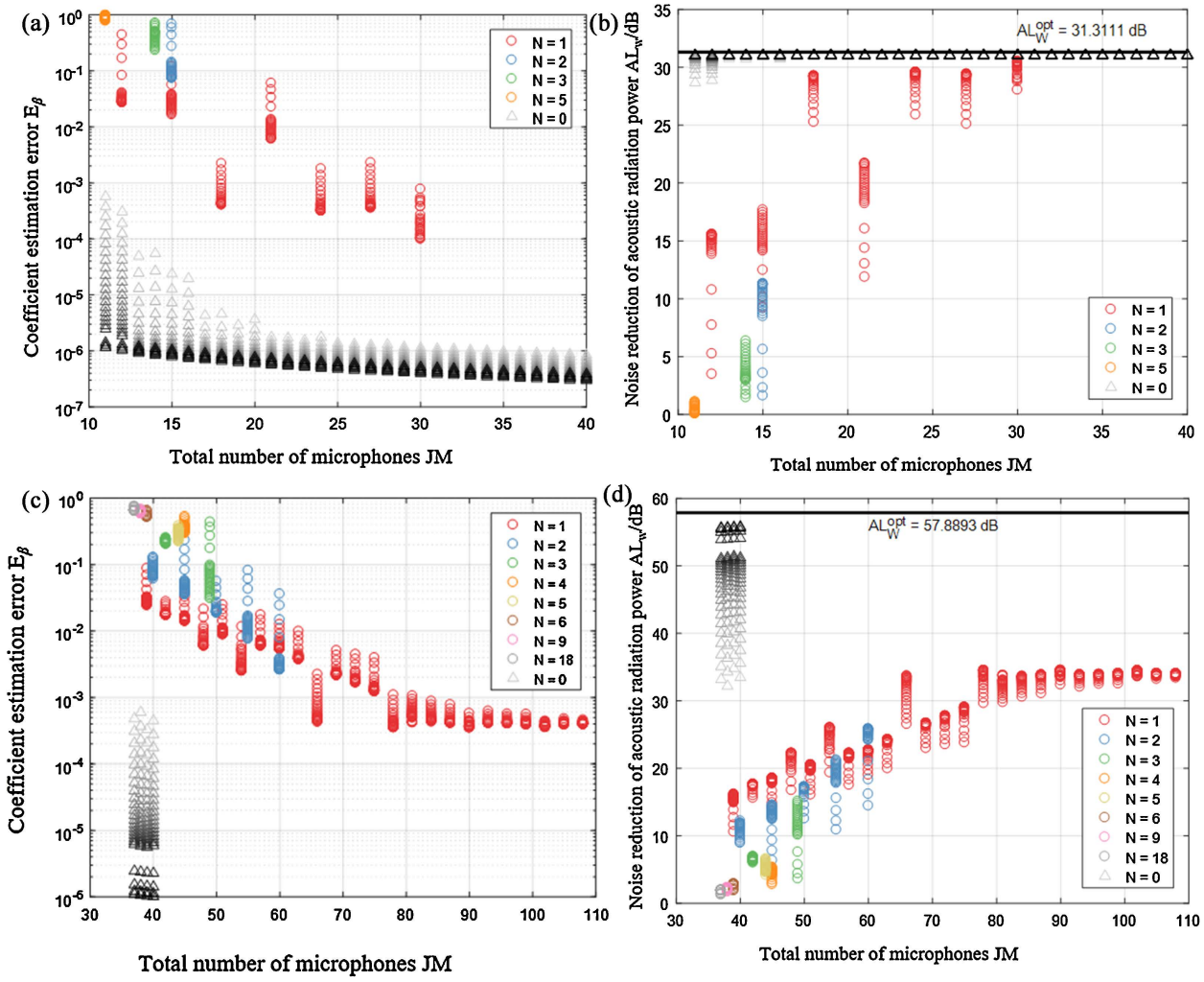

Figure 3. The relationship between the total number of microphones and the order of HOM and the coefficient estimation error and the noise reduction respectively. (a) 100 Hz; (b) 100 Hz; (c) 500 Hz; (d) 500 Hz.

5. Comparison with Sound Pressure Matching Strategy

In order to compare the performance of the wave domain strategy and the commonly used sound pressure matching strategy, in addition to the noise reduction AL_W, three system indicators are defined:

(1) Secondary sound source intensity energy SE

$$SE = \left\| \mathbf{q}_s \right\|^2. \tag{30}$$

Excessive SE will cause nonlinear response of the speaker, and long-time operation will damage the device.

(2) Secondary sound source intensity amplitude smoothness SM

$$SM = \frac{\overline{\rho}}{\mathrm{std}(\boldsymbol{\rho})} \tag{31}$$

where ρ is the amplitude of strength q_s, $\mathrm{std}(\cdot)$ represents the standard deviation. SM describes the degree of difference in the intensity amplitude of the

secondary sound source. In practice, it is hoped that the amplitude difference is small, that is, SM is large, so as to give full play to the role of each secondary sound source, which is conducive to system stability.

(3) The condition number κ of the system matrix

Wave domain strategy: $\kappa = \|\mathbf{\Gamma}\|\|\mathbf{\Gamma}^{-1}\|$; Sound pressure matching strategy:

$$\kappa = \|\mathbf{Z}\|\|\mathbf{Z}^{-1}\| \tag{32}$$

where $\mathbf{Z}$ is the ATI matrix from the secondary sound source position to the error sensor position. κ represents whether the system matrix is well-conditioned. If κ is large, the matrix is ill-conditioned, and the ANC system has poor robustness and is sensitive to external disturbances.

From the previous discussion, the error sensor selects the 0-order HOM, which is evenly distributed on the circumference from $\mathbf{O}_1 = (R_{\mathrm{HOM}}, \Delta\theta)$, where R_{HOM} reflects the distance between the error sensor and the secondary sound source, and 50 values are uniformly selected from $R_s + \lambda/1000$ to $R_s + \lambda/2$; the $\Delta\theta$ reflects the relative position of the error sensor layout and the secondary sound source layout, and 50 values are evenly selected from 0 to $2\pi/J$. At 100 Hz and 500 Hz, respectively, for the same electro-acoustic device layout (at 100 Hz, $M = 11$, $L = 9$; at 500 Hz, $M = 37$, $L = 29$), the noise reduction and three system indexes are calculated with the change of R_{HOM} and $\Delta\theta$, and the two strategies are used for control, as shown in **Figure 4** and **Figure 5**.

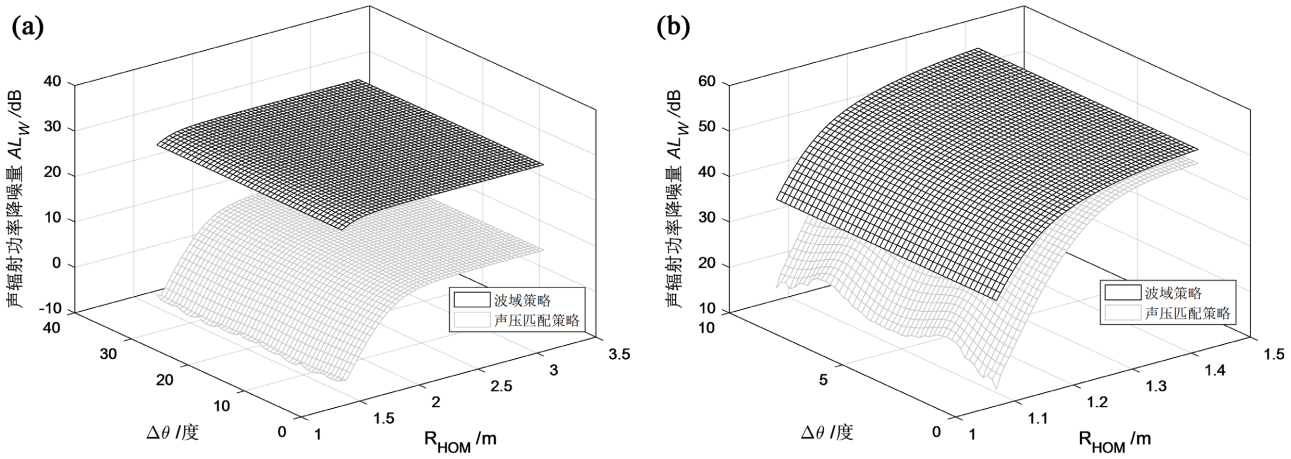

Figure 4. The noise reduction of the two strategies varies with R_{HOM} and $\Delta\theta$. (a) 100 Hz; (b) 500 Hz.

From **Figure 4**, it can be seen that the AL_W of the two strategies increases first with the increase of R_{HOM} (that is, the error sensor is far away from the secondary sound source), and then tends to be stable. The AL_W of the wave domain strategy is significantly larger than that of the sound pressure matching strategy, especially when the distance between the error sensor and the secondary sound source is very small, AL_W is close to the optimal noise reduction AL_W^{opt}. This is because the sum of the square of the sound field coefficient of the total sound field is closer to the total radiated sound power than the sum of the square of the sound

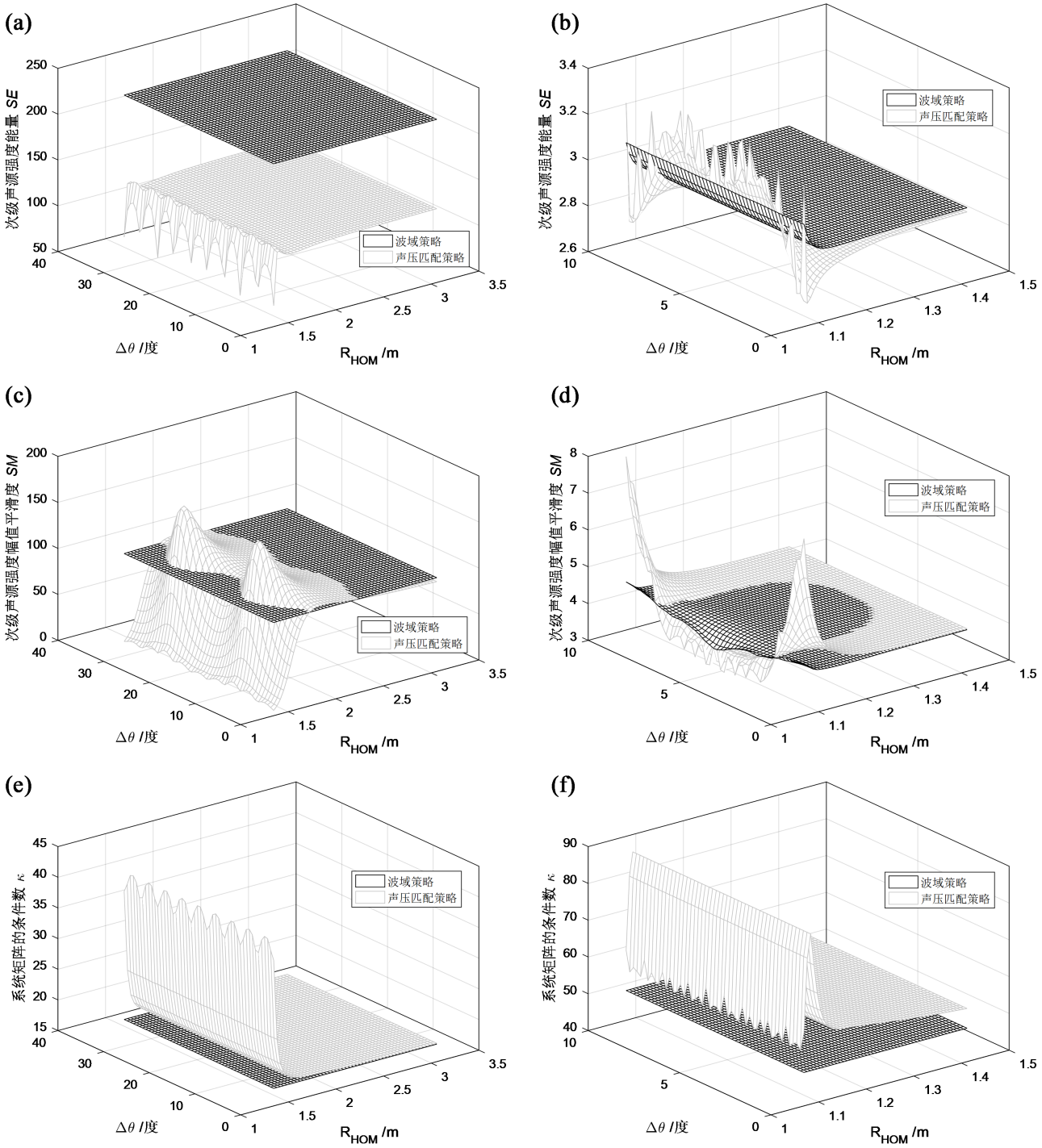

Figure 5. The system indices of the two strategies change with R_{HOM} and $\Delta\theta$. (a) 100 Hz (Strength energy); (b) 500 Hz (Strength energy); (c) 100 Hz (Strength amplitude smoothness); (d) 500 Hz (Strength amplitude smoothness); (e) 100 Hz (Condition number of system matrix); (f) 500 Hz (Condition number of system matrix).

pressure of the error point. From the perspective of control mechanism, the sound pressure matching strategy only performs inverse sound pressure matching on the primary sound field at the position of the error sensor, while the wave domain strategy controls the sound field basis function that contributes significantly, from

Equation (3), so that the sound pressure at any point in space is reduced, and the effect is closer to the goal of minimizing the total radiated sound power. It is found from **Figure 5** that the system index of the wave domain strategy is basically better than that of the sound pressure matching strategy, especially when the error sensor is close to the secondary sound source. In summary, the near-field sensing performance of the wave-domain strategy is better.

In addition, when R_{HOM} is very small, the AL_W and system index of the wave-domain strategy are almost unchanged with the change of $\Delta\theta$ (the relative position of the error sensor layout and the secondary sound source layout), while the sound pressure matching strategy is greatly affected by it. Because when the wave domain strategy is used, the driving sound of the secondary sound source is related to the layout of the secondary sound source and the estimated sound field coefficient, as shown in formula (18). The ATI coefficient matrix $\boldsymbol{\Gamma}$ contains only the secondary sound source layout information, which is different from the ATI matrix $\mathbf{Z}$ that contains both the secondary sound source layout and the error sensor layout information. The estimated sound field coefficient $\boldsymbol{\beta}_p$ is obtained by the error sensor picking up the sound pressure and then converted by Equation (9), which only involves the error sensor layout. Therefore, the error sensor layout and the secondary sound source layout are independent of each other, and the error sensor layout optimization only needs to pay attention to whether the sound field information is accurately picked up.

6. Conclusions

In this paper, a wave-domain near-field acoustic error sensing strategy is proposed. The equivalent relationship with the sound power minimization strategy and the optimal configuration parameters of the error sensor are explored, and compared with the sound pressure matching strategy. The research shows that:

(1) If there is no coefficient order truncation and coefficient estimation error, the proposed method is equivalent to the acoustic power minimization strategy.

(2) The best choice of error sensor is 0-order HOM, the number of which meets the minimum value of the overdetermined condition, and the position cannot be too close to the secondary sound source.

(3) When the error sensor is close to the secondary sound source, the wave domain strategy achieves better noise reduction performance ;

This feature can make the layout of the error sensor and the secondary sound source be optimized separately, which greatly simplifies the debugging workload of the layout optimization of the electroacoustic device in the project.

Conflicts of Interest

The authors declare no conflicts of interest regarding the publication of this paper.

References

[1] Nelson, P.A., Curtis, A.R.D., Elliott, S.J. and Bullmore, A.J. (1987) The Minimum

Power Output of Free Field Point Sources and the Active Control of Sound. *Journal of Sound and Vibration*, **116**, 397-414. https://doi.org/10.1016/s0022-460x(87)81373-1.

[2] Chen, K. (2014) Active Noise Control. 2nd Edition, National Defense Industry Press.

[3] Conover, W.B. (1956) Fighting Noise with Noise. *Noise Control*, **2**, 78-92. https://doi.org/10.1121/1.2369194

[4] Hesselmann, N. (1978) Investigation of Noise Reduction on a 100 kVA Transformer Tank by Means of Active Methods. *Applied Acoustics*, **11**, 27-34. https://doi.org/10.1016/0003-682x(78)90019-1

[5] Ross, C.F. (1978) Experiments on the Active Control of Transformer Noise. *Journal of Sound and Vibration*, **61**, 473-480. https://doi.org/10.1016/0022-460x(78)90449-2

[6] Gee, K.L. and Sommerfeldt, S.D. (2004) Application of Theoretical Modeling to Multichannel Active Control of Cooling Fan Noise. *The Journal of the Acoustical Society of America*, **115**, 228-236. https://doi.org/10.1121/1.1631940

[7] Wang, S., Sun, H., Pan, J. and Qiu, X. (2018) Near-Field Error Sensing for Active Directivity Control of Radiated Sound. *The Journal of the Acoustical Society of America*, **144**, 598-607. https://doi.org/10.1121/1.5049145

[8] Qiu, X., Hansen, C.H. and Li, X. (1998) A Comparison of Near-Field Acoustic Error Sensing Strategies for the Active Control of Harmonic Free Field Sound Radiation. *Journal of Sound and Vibration*, **215**, 81-103. https://doi.org/10.1006/jsvi.1998.1615

[9] National Technical Committee for Acoustic Standardization (2016) GB/T 3767-2016 Engineering Method for the Determination of Sound Power Level and Sound Energy Level of Noise Source by Acoustic Sound Pressure Method.

[10] Hansen, C., Snyder, S., Qiu, X., Brooks, L. and Moreau, D. (2012) Active Control of Noise and Vibration. CRC Press.

[11] Shafer, B.M., Gee, K.L. and Sommerfeldt, S.D. (2010) Verification of a Near-Field Error Sensor Placement Method in Active Control of Compact Noise Sources. *The Journal of the Acoustical Society of America*, **127**, EL66-EL72. https://doi.org/10.1121/1.3272632

[12] Li, H., Chen, K. and Sun, J. (1999) Optimal Placement of Adaptive Active Noise Elimination Error Sensor in Free Sound Field. *Journal of Northwestern Polytechnical University*, **17**, 29-33.

[13] Martin, T. and Roure, A. (1998) Active Noise Control of Acoustic Sources Using Spherical Harmonics Expansion and a Genetic Algorithm: Simulation and Experiment. *Journal of Sound and Vibration*, **212**, 511-523. https://doi.org/10.1006/jsvi.1997.1444

[14] Liu, J. and Ying, L. (2014) Optimization of Active Control System for Power Transformer Noise Based on Particle Swarm Optimization. *Journal of Wuhan University* (*Engineering Edition*), **47**, 498-501.

[15] Samarasinghe, P.N., Abhayapala, T.D. and Poletti, M.A. (2011) Spatial Sound Field Recording over a Large Area Using Distributed Higher Order Microphones. 2011 *IEEE Workshop on Applications of Signal Processing to Audio and Acoustics* (*WASPAA*), New Paltz, 16-19 October 2011, 221-224. https://doi.org/10.1109/aspaa.2011.6082297

[16] Samarasinghe, P.N., Abhayapala, T.D. and Poletti, M. (2014) Wavefield Analysis over Large Areas Using Distributed Higher Order Microphones. *IEEE/ACM Transactions on Audio, Speech, and Language Processing*, **22**, 647-658. https://doi.org/10.1109/taslp.2014.2300341

[17] Wang, Y., Chen, K., Yu, H. and Xu, J. (2018) Spherical Harmonic Function Decomposition and Sound Field Reconstruction of Low-Frequency Sound Field in Cylindrical Cavity. *Acoustic Journal*, **43**, 719-727.

[18] Zhang, J., Abhayapala, T.D., Zhang, W., Samarasinghe, P.N. and Jiang, S. (2018) Active Noise Control over Space: A Wave Domain Approach. *IEEE/ACM Transactions on Audio, Speech, and Language Processing*, **26**, 774-786. https://doi.org/10.1109/taslp.2018.2795756

[19] Zhang, W., Hofmann, C., Buerger, M., Abhayapala, T.D. and Kellermann, W. (2018) Spatial Noise-Field Control with Online Secondary Path Modeling: A Wave-Domain Approach. *IEEE/ACM Transactions on Audio, Speech, and Language Processing*, **26**, 2355-2370. https://doi.org/10.1109/taslp.2018.2864577

[20] Watson, G.N. (1995) A Treatise on the Theory of Bessel Functions. Cambridge University Press.

[21] Williams, E. (1999) Fourier Acoustics: Sound Radiation and Nearfield Acoustic Holography. Academic Press.

[22] Zeng, Y., Zheng, Y., Jin, Z., *et al.* (2024) Fault Location Method of Power Equipment Based on MF-DNN Algorithm Using Acoustic Signal. *Guangdong Electric Power*, **37**, 64-71.

[23] Zhao, Z., Huang, J., Wang, Y., *et al.* (2024) Dynamic State Estimation of Generators Based on CKMC-CKF under Non-Gaussian Noise. *Guangdong Electric Power*, **37**, 115-122.